Bio-Design and Manufacturing (2024) 7:57–73
https://doi.org/10.1007/s42242-023-00249-z

RESEARCH ARTICLE

Constructing a biofunctionalized 3D-printed gelatin/sodium alginate/chitosan tri-polymer complex scaffold with improvised biological and mechanical properties for bone-tissue engineering

Amit Kumar Singh[1] · Krishna Pramanik[1] · Amit Biswas[1]

Received: 5 January 2023 / Accepted: 7 June 2023 / Published online: 13 December 2023

Abstract
Sodium alginate (SA)/chitosan (CH) polyelectrolyte scaffold is a suitable substrate for tissue-engineering application. The present study deals with further improvement in the tensile strength and biological properties of this type of scaffold to make it a potential template for bone-tissue regeneration. We experimented with adding 0%–15% (volume fraction) gelatin (GE), a protein-based biopolymer known to promote cell adhesion, proliferation, and differentiation. The resulting tri-polymer complex was used as bioink to fabricate SA/CH/GE matrices by three-dimensional (3D) printing. Morphological studies using scanning electron microscopy revealed the microfibrous porous architecture of all the structures, which had a pore size range of 383–419 μm. X-ray diffraction and Fourier-transform infrared spectroscopy analyses revealed the amorphous nature of the scaffold and the strong electrostatic interactions among the functional groups of the polymers, thereby forming polyelectrolyte complexes which were found to improve mechanical properties and structural stability. The scaffolds exhibited a desirable degradation rate, controlled swelling, and hydrophilic characteristics which are favorable for bone-tissue engineering. The tensile strength improved from (386±15) to (693±15) kPa due to the increased stiffness of SA/CH scaffolds upon addition of gelatin. The enhanced protein adsorption and in vitro bioactivity (forming an apatite layer) confirmed the ability of the SA/CH/GE scaffold to offer higher cellular adhesion and a bone-like environment to cells during the process of tissue regeneration. In vitro biological evaluation including the MTT assay, confocal microscopy analysis, and alizarin red S assay showed a significant increase in cell attachment, cell viability, and cell proliferation, which further improved biomineralization over the scaffold surface. In addition, SA/CH containing 15% gelatin designated as SA/CH/GE_{15} showed superior performance to the other fabricated 3D structures, demonstrating its potential for use in bone-tissue engineering.

Keywords Scaffold · Biomaterial · Sodium alginate · Chitosan · Gelatin · 3D printing · Tissue engineering

Introduction

Tissue engineering is a promising approach for curing diseased or damaged bone tissue by providing a biologically functionalized substitute [1]. In this technique, an artificial extracellular matrix (ECM) called a scaffold acts as a platform for the attachment, growth, and proliferation of cells [2–4]. Researchers have developed numerous artificial polymeric ECM structures to support cell attachment and growth, as well as direct differentiation for regenerating damaged tissues [5]. The selection of appropriate biopolymers for scaffold development is a pivotal task in bone-tissue engineering (BTE). Biomaterials are selected based on their biodegradability, biocompatibility, wettability, mechanical strength, hydrophilicity, and bioactivity [6, 7]. Biopolymers such as chitosan (CH) [8], sodium alginate (SA) [9], gelatin (GE) [10], silk [11], agarose [12], carboxymethyl cellulose [13], polycaprolactone [14], polyvinyl alcohol [15], polyethylene oxide [16], and pectin [17] have been widely used for BTE. Among these, sodium alginate, chitosan, and gelatin have attracted much attention for BTE application.

Sodium alginate, an anionic polysaccharide comprised of β (1–4)-linked D-mannuronic acid (M) and α (1–4)-linked L-guluronic acid (G), and uronic acids, is derived from brown seaweed [18–21]. It has been extensively investigated in different fields like food technology, membrane

✉ Krishna Pramanik
kpr@nitrkl.ac.in

[1] Centre of Excellence in Tissue Engineering, Department of Biotechnology and Medical Engineering, National Institute of Technology, Rourkela 769008, India

design, drug delivery, and tissue engineering because it offers several favorable properties such as hydrophilicity, biodegradability, biocompatibility, low cost, rapid gel formation, and easy availability [22–26]. SA is an excellent biopolymer for in vitro as well as in vivo application [27]. Chitosan, a natural polymer, is extracted by partial deacetylation of the chitin present in the exoskeletons of crabs, lobsters, shrimp, and similar marine creatures [28]. Chitosan consists of poly(β-(1–4)-linked-2-amino-2-deoxy-O-glucose) and a linear polysaccharide with a β-1,4-linked polymer of glucosamine (2-amino-2-deoxy-β-D-glucose) and N-acetylglucosamine and 1–4 glycosidic bonds [29–32]. Its unique combination of properties such as biodegradability, non-toxicity, biocompatibility, hemostatic activity, anti-inflammatory activity, and antimicrobial activity makes it an ideal material for tissue engineering [33–35]. Its bioactivity is due to the presence of amino groups on its hydrophilic surface which promote cell adhesion and proliferation, differentiation of osteoblast cells, and bone mineralization [29, 36]. Chitosan has also been used in many other applications, for example wound healing [37], antibacterial activity [38], and drug delivery [39]. Blending the negatively charged carboxylic group of sodium alginate and the positively charged amines of chitosan forms a polyelectrolyte complex (PEC) which improves the mechanical properties of the polymeric blend and provides structural stability during in vivo implantation [40–42]. PEC also provides a superior surface that is favorable for the cell attachment, proliferation, as well as an ideal microenvironment for bone-tissue regeneration [41]. In our previous study [43], we used bioink prepared from an SA/CH-blend polyelectrolyte to fabricate three-dimensional (3D)-printed scaffold with a desired set of properties; that was proven to be a suitable template for tissue-engineering application. However, the mechanical and biological properties of the scaffold would need to be improved to make it suitable for BTE.

Gelatin, which is derived from collagen, is a widely recognized natural biopolymer for scaffold fabrication [44]. In spite of low antigenicity compared to its parent source, gelatin contains some informational signals like a unique RGD (arginine–glycine–aspartic) sequence similar to that of collagen amino acids such as glycine, proline, and hydroxyproline; these promote cell adhesion, proliferation, and differentiation [45–47]. Gelatin is biocompatible, biodegradable, hemocompatible, low-cost, easily available, and non-toxic in nature [44, 48, 49]. The peptide sequence present in GE helps cell integrin to adhere on the scaffold surface, thereby promoting cell adhesion, migration, proliferation, and differentiation [14]. Gelatin has been blended with various polysaccharides and other biopolymers (for example alginate and chitosan) to improve their biological and mechanical properties [9, 50]. However, the combined effect of the SA/CH blend and gelatin as a 3D-printed ECM has not yet been investigated for bone-tissue regeneration. Although both alginate and chitosan have their own advantages such as biocompatibility, biodegradability, bioactivity, hydrophilicity, hemocompatibility, or non-toxicity which are useful properties for BTE, incorporating gelatin into the SA/CH scaffold provides an informational signal due to the presence of the arginine–glycine–aspartic acid sequence, which may enhance the biological properties of the bulk scaffold [22, 51–54]. Therefore, we hypothesized before commencing our study that the addition of gelatin might improve the tensile strength and biological properties of SA/CH scaffold, thereby making it a potential template for cell attachment and proliferation, and further, for bone-tissue regeneration.

In addition to the choice of ideal biopolymers, the fabrication method plays a vital role in manufacturing a scaffold with the desired shape, size, and microstructure. The goal is to produce anatomically and physiologically hierarchical 3D network structures similar to the native bone ECM. Remarkable advances in fabrication techniques have been achieved in recent years in terms of manufacturing scaffolds with a 3D design and the desired architecture. 3D printing is the most promising fabrication method and has attracted much attention because of its capacity to fabricate scaffolds of specific size, shape, and design. The resulting scaffolds have the desired microstructure that mimics the defective tissue [55] and are reproducible; hence, they have been widely used in recent years [56]. Fabrication of a scaffold in one step, using a 3D dataset and without the need for a mold, is another advantage of this technique [57]. Therefore, our aim was to construct a 3D-printed SA/CH/GE tri-polymer complex structure with improved mechanical and biological properties for BTE application. To the best of our knowledge, this is the first report on an investigation of the effects of gelatin on the properties of SA/CH scattfold. 3D-printed SA/CH/GE scaffold with optimized composition and structure would provide an appropriate bioactive microenvironment for bone-tissue regeneration.

Materials and methods

Preparation of SA/CH/GE bioink

Sodium alginate, chitosan, and gelatin from HIMEDIA were used in this study. Sodium alginate solution (2%, mass fraction) was prepared in distilled water and chitosan solutions (1.5%, mass fraction) were prepared in 2% (volume fraction) acetic acid solution. The polymer solutions were blended in a 60:40 volume ratio. The solution of gelatin (0.1 g/mL), prepared by dissolving 5 g gelatin in 50 mL distilled water at 40 °C, was mixed with SA/CH blend in different volume ratios in the range of 0%–15%, resulting in tri-polymer blends which we represented as SA/CH/GE_5,

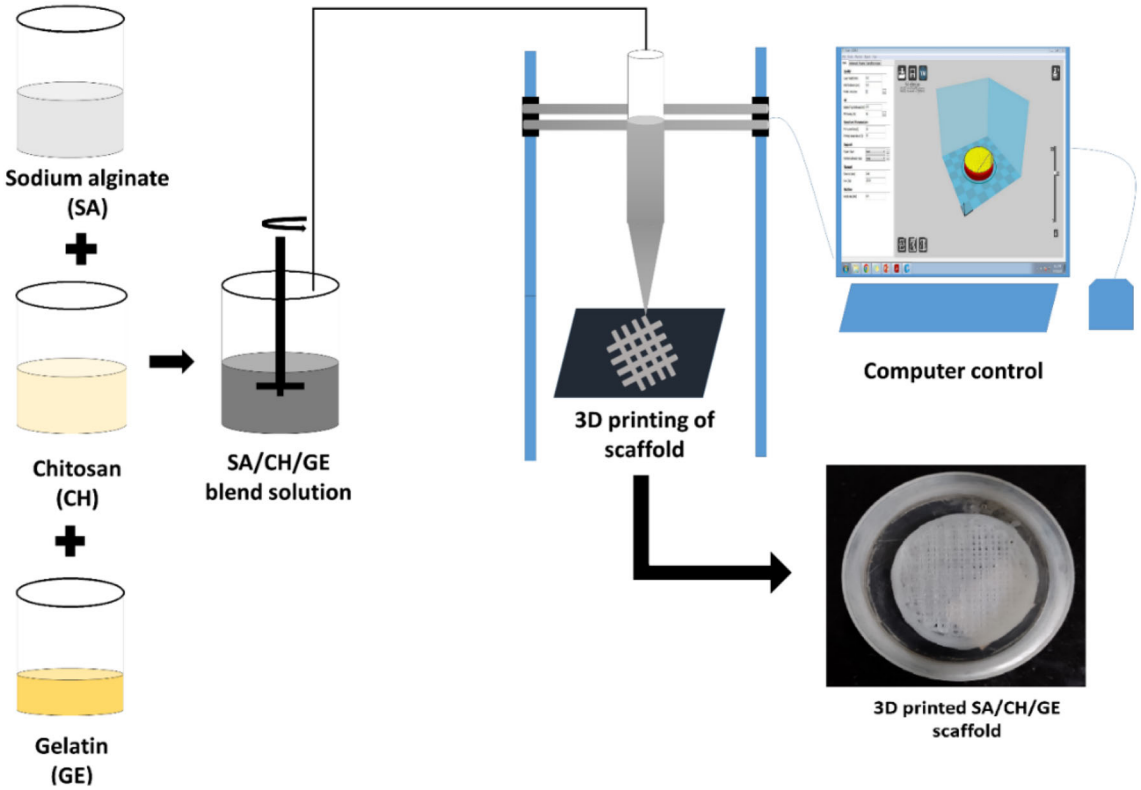

Fig. 1 Steps of the 3D printing process. The first step: blending of SA and CH to prepare the SA/CH blend. Second step: addition of gelatin solutions to the SA/CH blend, resulting in SA/CH/GE tri-polymeric bioinks. Final step: printing of the bioinks using a computer-controlled 3D printer to fabricate microfibrous scaffolds. SA: sodium alginate; CH: chitosan; GE: gelatin

$SA/CH/GE_{10}$, and $SA/CH/GE_{15}$. For crosslinking of the 3D-printed SA/CH/GE scaffolds, 1.36 mol/L aqueous calcium chloride solution and 3% (mass fraction) 1-ethyl-3-(3-dimethylaminopropyl)carbodiimide (EDC)/N-hydroxysuccinimide (NHS) (2/1 (mass ratio)) in 95% ethanol solution (95/5) were prepared.

Fabrication of 3D-printed scaffold

We used a laboratory-built 3D printer to fabricate scaffolds from SA/CH and SA/CH/GE bioinks. The printer consisted of a platform and a printer head that were movable along the *x*, *y*, and *z* axes. A 15 mL dispensing tube (0.8 mm nozzle diameter) was connected to the printer head and moved along with it. A stepper motor with a 1.8° step angle controlled the movement of the printer head and the platform. The printing device was operated and controlled by Cura software (Ultimaker), an open-source software.

A 3D model created using Solid Works 2012 was saved in '.STL' format and then sliced into two-dimensional (2D) layers using Cura software (version: 15.04); G-codes were also generated. The dispenser was filled with the prepared bioinks for printing with optimized parameters (10 mm/min printing speed, 40% fill density, and 0.6 mm layer height). The platform moved along the *x* and *y* axes according to the G-codes. After completion of one layer, the printer head moved along the *z*-axis according to the layer height and printed another layer. For fast gelling, we kept the 3D-printed microfibrous scaffold in calcium chloride in a petri dish placed over the platform, just below the nozzle tip. The printed scaffolds were left for one hour in the calcium chloride solution, and then washed thoroughly with distilled water to remove excess calcium chloride. The scaffolds were then crosslinked with EDC-NHS solution for 24 h at 4 °C (to crosslink the gelatin), followed by thorough washing with distilled water to remove any excess EDC-NHS. Finally, the printed scaffolds were dried by lyophilization. Figure 1 shows the schematic diagram of 3D printing of SA/CH/GE scaffold.

Characterization

Rheological study of printing ink

The viscosity of the tri-polymeric blend solutions was measured using a Viscometer Bohlin Visco-88 from Malvern. We placed the polymeric blend solutions between the rotational

cone and platform and measured their viscosity at varying shear rates in the range of 21–1066 s^{-1}, at room temperature. We then created and analyzed the viscosity–shear rate graph.

Scanning electron microscopy

The microfibrous porous structures of the 3D-printed scaffolds were seen using scanning electron microscope (SEM, JEOL JSM- 6480 LV). Small, square pieces of scaffold were placed over the stub using carbon tape. After 5 min of platinum coating, we subjected the scaffolds to SEM imaging. The images were captured at different magnifications at 20 kV. We analyzed the fiber diameter and pore size of the scaffolds using ImageJ software.

X-ray diffraction (XRD)

We obtained XRD images of the scaffolds using an X-ray diffractometer (Rigaku Ultima-IV, Japan). Small pieces of the scaffolds were placed over the specimen holder and exposed to X-ray light. The reflected rays were recorded for further analysis. The XRD spectra of the scaffolds were recorded between 2θ=10° and 60° with a step size of 0.002 at 10°/min [58].

Fourier-transform infrared spectroscopy (FTIR)

FTIR spectra of the 3D-printed scaffolds were recorded in transmittance mode using FTIR equipment from Shimadzu AIM-8800, Japan. The spectra were observed within the mid-infrared region (500–4500 cm^{-1}). We ground a tiny amount of each scaffold with potassium bromide and pressed it into pellets; we then exposed these to infrared light and recorded the spectrum [59].

Contact angle

Measuring the contact angle of the 3D-printed scaffold was quite difficult due to the large and regular patterned pore structure, which allowed smooth flow of water drops through the material. For this reason, we cast the printing inks in the form of film and crosslinked them with calcium chloride, as well as EDC-NHS. The films were used to measure the contact angle using a drop shape analyzer (Kruss DSA 25), by subtending a drop of water over the film surface [60].

Swelling study

We examined the swelling properties of the 3D-printed scaffold structures in simulated body fluid (SBF) which was prepared by following a procedure described elsewhere [43, 61]. After recording initial dry weights (W_d), we treated the scaffolds with SBF at 37 °C. At a predetermined time interval, we removed the swollen scaffolds and a trace amount of SBF from them by soaking it up with filter paper. Then, we measured the final weight (W_s) of the scaffolds and calculated the amount of swelling (%) using the following formula [62]:

$$\text{Swelling} = \frac{W_s - W_d}{W_d} \times 100\%.$$

Degradation study

Degradation studies of the prepared 3D-printed scaffolds were performed by following a protocol described elsewhere [63]. The pre-weighted scaffolds were treated with SBF solution for a fixed time period at 37 °C. After particular time intervals, the scaffolds were taken out of the SBF and washed thoroughly to remove deposited salt. The degraded scaffolds were dried in an oven. The weight of the scaffold before degradation was denoted as W_o, and after degradation was denoted as W_t. The degradation was calculated with the following formula:

$$\text{Degradation} = \frac{W_o - W_t}{W_o} \times 100\%.$$

In vitro bioactivity

We performed in vitro bioactivity tests on the fabricated 3D-printed scaffolds by exposing them to SBF solution. Scaffolds were exposed to SBF for 7 d at 37 °C with the SBF changed every 48 h during the study period. After 7 d, the samples were removed from the SBF and gently washed with distilled water, followed by lyophilization [63]. We characterized the freeze-dried samples to confirm their apatite-layer formation. SEM was used to observe the morphology of the deposited apatite layer and XRD was performed to confirm the phase of the apatite layer formed over the scaffold surface.

Mechanical test

The tensile strength of the 3D-printed scaffolds was assessed using a universal testing machine (UTM, Instron 3369, Bioplus, USA). We prepared all scaffolds with seven bioink layers, and small pieces of the scaffolds (25 mm×5 mm) were placed between the clasps of the UTM. The tensile test was done using a 250-N load cell at a cross-head speed of 1 mm/min.

Protein adsorption

We conducted protein-adsorption studies to evaluate the bovine serum albumin (BSA) protein adsorption over each scaffold surface [64]. The 3D-printed scaffolds were immersed in a BSA solution comprised of 1 mg/mL BSA protein in phosphate-buffered saline (PBS of Gibco make) and incubated for 24 h at 37 °C. A Bradford assay was performed to analyze the protein adsorption. After incubation, 30 μL of supernatant solution taken from each sample was mixed with Bradford reagent (purchased from Sigma-Aldrich). The absorbance was recorded at 595 nm using a spectrophotometer (Systronix, double-beam spectrophotometer 2203). The amount of residual BSA protein in the supernatant was measured against the standard graph of BSA protein created by plotting the absorbance in a BSA concentration range of 0.1–1 mg/mL. Finally, we calculated the amount of protein adsorbed over the scaffold surface by subtracting the remaining BSA protein in the supernatant from the initial amount.

Biological characterization

In vitro cell culture Osteoblast-like cells (Saos-2 cells) isolated from human osteosarcoma tissue were purchased from the National Centre for Cell Science, Pune, India, and cultured in complete culture media (CCM) comprised of 85% Dulbecco's modified Eagle medium, 15% fetal bovine serum, and 1% antibiotic antimycotic solution from HIMEDIA LAB. After cells reached 80%–90% confluence, trypsin was added for 5–10 min to remove the cells from the flask surface. The trypsinized cells were collected in a tube with complete culture medium and centrifuged at 5000 r/min for 10 min. The cell pellet formed was dispersed in complete culture medium. Then, we used the cell suspension for the in vitro cell study.

Scaffolds with dimensions of 1 cm × 1 cm were sterilized with 70% ethanol followed by washing three times with 1× PBS. The scaffolds were incubated in CCM for 10–12 h at 37 °C. After removing the medium, the cells were seeded on the scaffolds. The cell-seeded scaffolds were incubated for 4–6 h at 37 °C in a 5% CO_2 environment for initial cell attachment, followed by culturing in complete culture medium for 7 d at 5% CO_2 and 37 °C in a humid environment.

MTT assay We performed MTT assays on the 3D-printed scaffolds over a period of 5 d. The Saos-2 cells (with a cell density of 1×10^4 cells/cm^2) were seeded over the scaffolds and cultured for 5 d. After 1, 3, and 5 d of culture incubation, the medium was discarded and the constructs were washed with PBS. MTT (3-[4,5-dimethylthiazole-2-yl]-2,5-diphenyltetrazolium bromide) reagent (0.5 mg/mL) was prepared and 100 μL was added to each well; the next step was incubation in a 5%-CO_2 environment for 4 h at 37 °C. The MTT solution was removed from each well and 100 μL dimethyl sulfoxide was poured to dissolve the purple formazan crystal that had formed. We recorded the absorbance using an ultraviolet (UV)-visible spectrophotometer at 490 nm [65–67].

Cell morphology and cytoskeleton organization We observed the morphology of the cells in the construct under SEM and inspected their cytoskeleton organization by confocal microscopy. For SEM study, the scaffolds were seeded with Saos-2 osteoblast-like cells (1×10^5 cells/cm^2) and cultured for a period of one week. After the fourth and seventh days, the medium was removed from the wells and the cells were fixed by treatment with 2.5% glutaraldehyde solution for 20 min; cells were then washed several times using graded aqueous ethanol (30%–100%) and finally dried at room temperature [68].

For confocal microscopic analysis, we fixed the cells in the construct using 4% paraformaldehyde solution and then incubated them with 3% BSA solution for 30 min. The constructs were permeabilized by treatment with 0.1% triton X-100 for 5 min. We added Alexa-Fluor 488 conjugated phalloidin to the cell-seeded scaffolds and kept them for 15 min at room temperature. The constructs were washed three times with PBS and 4′,6-diamidino-2-phenylindole (DAPI) staining solution was then added; kept for 15 min in order to stain the nuclei. This was followed by washing with PBS to remove excess staining solution. We visualized the stained constructs with a confocal microscope (Leica TCS SP5 X Super continuum).

In vitro biomineralization In vitro biomineralization of the 3D-printed scaffolds was assessed by alizarin red S (ARS) assay. The scaffolds were seeded with Saos-2 osteoblast-like cells and cultured for 7 d. ARS staining solution (2%, mass fraction) prepared by dissolving the ARS powder in Milli-Q water was adjusted to a pH between 4.1 and 4.3, using 10% NaOH solution. After seven days of cell culture, the constructs were thoroughly washed with PBS and the cells were fixed by treating with 4% paraformaldehyde solution, followed by washing with PBS. Staining solution (1 mL) was added to the construct and it was incubated for 1 h at 37 °C. The residual amount of ARS solution was removed by repeated washing with Milli-Q water. We performed a qualitative analysis of biomineralization by capturing images of ARS-stained constructs with an inverted-phase contrast microscope. For quantitative measurement, the stained scaffolds were immersed in 700 μL of a 10% acetic acid solution to solubilize the ARS stain for 5 min, and optical density (OD) was then measured at 405 nm using UV–vis spectroscopy [69].

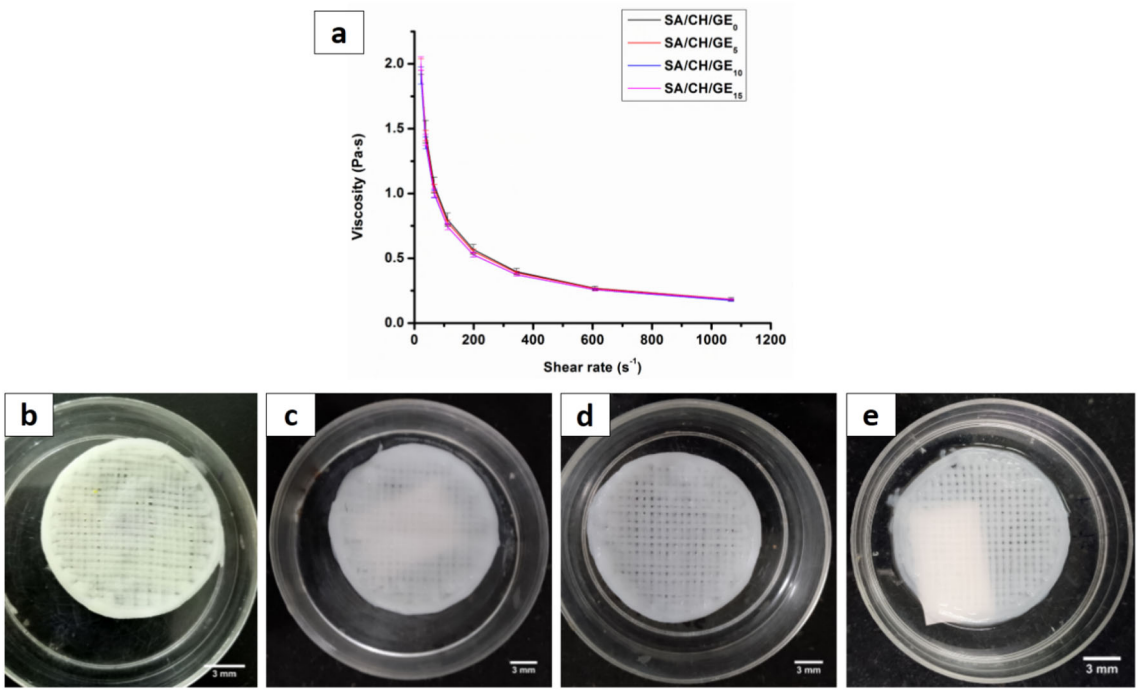

Fig. 2 **a** Rheological behavior of the SA/CH/GE printing solutions. **b–e** Optical images of the fabricated SA/CH/GE scaffolds with varying gelatin content (0%–15%), **b** $SA/CH/GE_0$ used as control, **c** $SA/CH/GE_5$, **d** $SA/CH/GE_{10}$, and **e** $SA/CH/GE_{15}$. SA: sodium alginate; CH: chitosan; GE: gelatin

Statistical analysis All quantitative results are presented in terms of mean±standard deviation (SD). The statistical analysis of the experimental results was done with GraphPad Prism 8 using one- and two-way analysis of variance (ANOVA) tests, and the statistical significance is represented as $^{*}p<0.05$, $^{**}p\leq0.01$, $^{***}p\leq0.001$, and $^{****}p\leq0.0001$ [70–73].

Results and discussion

Rheological behavior of bioinks

The rheological behavior of a polymeric solution is an important factor in 3D printing. Rheological properties are determined by measuring viscosity at varied levels of shear stress, which helps to determine the flow of printing ink from the dispensing nozzle of a 3D printer [74]. We recorded the viscosity of the prepared printing inks, comprised of SA/CH/GE blends with varying gelatin content (0%–15%, volume fraction) at different shear rates (Fig. 2a). As indicated, there was no significant change in the viscosity of the SA/CH blends upon the addition of gelatin, and the same viscosity pattern was obtained with all composition of SA/CH/GE blends. The viscosity of the printing inks decreased as the shear rate increased, confirming their shear-thinning characteristics; these were due to disentanglement of the polymeric network [75]. The shear-thinning property shows the great potential of printing with tri-polymeric inks for scaffold fabrication [76].;

Fabrication of 3D-printed SA/CH/GE scaffolds

We used the prepared SA/CH/GE blends (with varying gelatin content in the range of 0%–15%) as printing inks, and successfully fabricated microfibrous scaffolds with 3D architecture by 3D printing. The scaffolds were designated as $SA/CH/GE_0$, $SA/CH/GE_5$, $SA/CH/GE_{10}$, and $SA/CH/GE_{15}$, respectively. We did not observed structural fidelity during the printing with the (SA/CH)/GE: 80/20 ($SA/CH/GE_{20}$) ink. The optical images of the scaffolds are displayed in Figs. 2b–2e. The scaffolds were fabricated with layer-by-layer assembly by the extrusion of SA/CH/GE polymeric blends from the dispenser (as described above), and calcium chloride solution was used to instantly gel the printed structures, which were further crosslinked with EDC-NHS solution.

Morphological analysis

We analyzed the surface morphology of the fabricated scaffolds by assessing the SEM images. Figure 3 displays

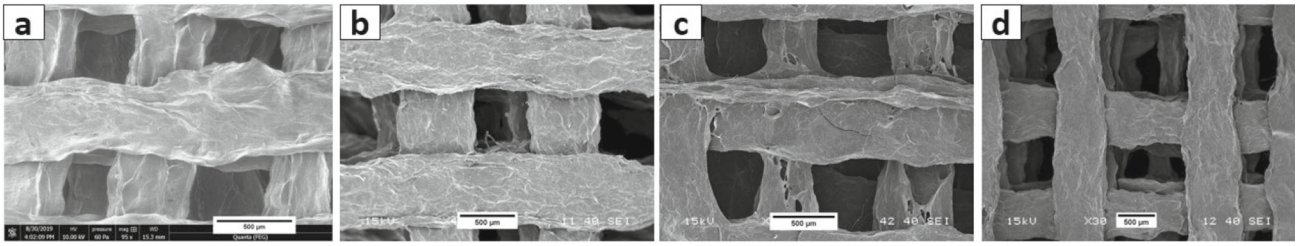

Fig. 3 SEM images of the 3D-printed SA/CH/GE structures with varying gelatin content. **a** $SA/CH/GE_0$ (control), **b** $SA/CH/GE_5$, **c** $SA/CH/GE_{10}$, and **d** $SA/CH/GE_{15}$. Scale bars: 500 μm. SEM: scanning electron microscopy; SA: sodium alginate; CH: chitosan; GE: gelatin

the microfibrous and microporous open pore structures of all compositions of the scaffold, which exhibited a more or less square shape and an interconnected pore network. The gelatin concentration in the SA/CH scaffold had a significant impact on pore size and fiber diameter. However, no significant change in surface morphology was observed, among the scaffolds with varying gelatin content. The fiber diameter of the scaffolds increased with gelatin content, and the values were (369±42), (519±50), (565±94), and (578±61) μm with $SA/CH/GE_0$, $SA/CH/GE_5$, $SA/CH/GE_{10}$, and $SA/CH/GE_{15}$, respectively. The pore sizes of the scaffolds, (383±92), (431±91), (439±98), and (491±115) μm, for $SA/CH/GE_0$, $SA/CH/GE_5$, $SA/CH/GE_{10}$, and $SA/CH/GE_{15}$, respectively, were observed to be suitable for bone-tissue engineering, which requires a pore-size ranging from 20 to 1500 μm [54]. The similar pore sizes we measured indicate the rigid and stable structure of the scaffolds resulting from crosslinking of gelatin in the SA/CH/GE with EDC-NHS [77].

Chemical composition analysis

We performed FTIR analysis to determine the functional groups of respective polymers and thus chemical composition of the scaffolds. Figure 4 displays the FTIR spectra of $SA/CH/GE_0$ scaffolds (Fig. 4a) as well as pure GE, $SA/CH/GE_5$, $SA/CH/GE_{10}$, and $SA/CH/GE_{15}$ scaffolds (Fig. 4b). In FTIR spectra of $SA/CH/GE_0$, the characteristic peaks at 818 and 890 cm^{-1} indicated the occurrence of β-glycosidic linkage between the glucuronic acid and mannuronic acid of the alginate [78, 79]. C–OH, C–O–C, and C–O groups were observed at 1156 cm^{-1}, whereas C–H bending was found at 1400 cm^{-1}. The peak found around 1600 cm^{-1} corresponds to the formation of polyelectrolyte complex between carboxylic groups of alginate and amine groups of chitosan [80]. In the FTIR spectra of pure gelatin (Fig. 4b), the characteristic bands at 3285 and 3073 cm^{-1} indicated N–H stretching of amide II. We ascribed the absorbance at 2940 cm^{-1} to stretching of alkyl groups of C–H. The characteristic bands at 1243, 1544, and 1650 cm^{-1} were due to N–H stretching of amides I–III [81].

In the FTIR spectra of SA/CH/GE-blend scaffolds (Fig. 4b), we observed the main characteristic bands with small shifts. The C–H bending vibration was found at 1387, 1388, and 1385 cm^{-1} (with small shifts) in the $SA/CH/GE_5$, $SA/CH/GE_{10}$, and $SA/CH/GE_{15}$ scaffolds, respectively, in comparison to pure chitosan (1378 cm^{-1}) and gelatin (1395 cm^{-1}) [82]. Furthermore, the carboxyl asymmetric stretching vibration for $SA/CH/GE_5$, $SA/CH/GE_{10}$, and $SA/CH/GE_{15}$ was found at 1644, 1631, and 1634 cm^{-1} respectively, with small shifts from 1608 cm^{-1}. These shifts may have been due to overlapping of the corresponding amide I of chitosan and gelatin. The N–H stretching was shifted to around 3400 cm^{-1} in all the SA/CH/GE scaffolds [83]. The shifting of absorbance bands represents the internal polymeric reaction between the alginate, chitosan, and gelatin.

XRD analysis

XRD analysis was performed to assess the phase composition and crystallinity of the 3D-printed scaffolds [84]. The XRD spectra recorded in the range of 2θ=10°–60° are displayed in Fig. 5, wherein $SA/CH/GE_0$ spectra used as control were referred from our previous work [43]. As is shown, the gelatin added to the SA/CH blend did not affect the phase of the scaffold, and invariably a wide peak observed from 2θ=20° to 35° in the XRD spectra confirmed the amorphous nature of all the scaffold compositions, thereby demonstrating their suitability for tissue engineering. Alginate and gelatin are amorphous [85, 86], whereas chitosan is crystalline in nature [87]. The XRD spectrum of the SA/CH/GE-blend scaffolds is wide, without the presence of any obvious crystal peak; this could be attributed to the fact that the blending of these polymers might have distorted the hydrogen bonding between the hydroxyl and amino groups of chitosan [65, 88]. Scaffolds in an amorphous phase are expected to show superior cytocompatibility and cell-proliferation activities in comparison to scaffolds in a crystalline state [89].

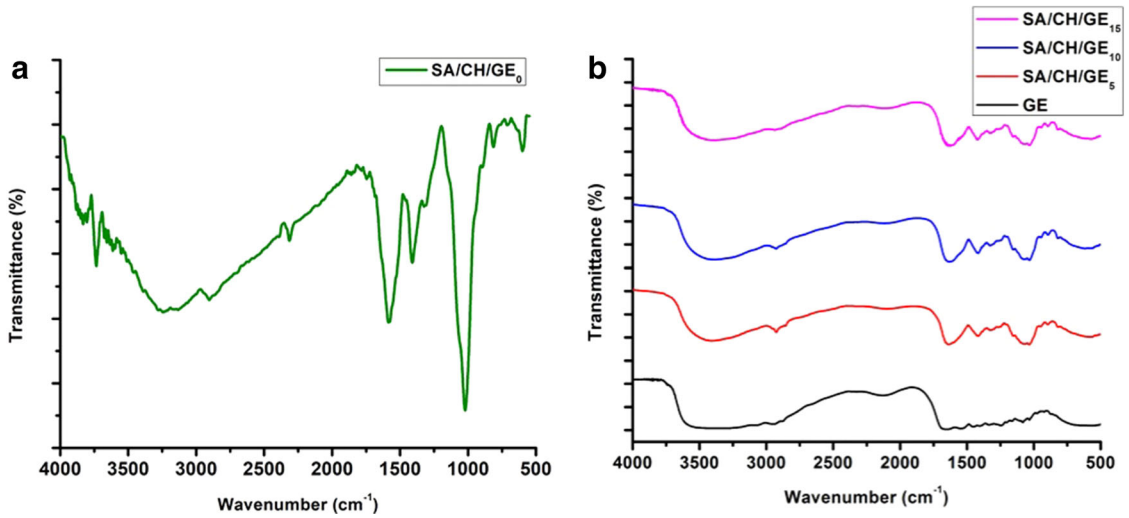

Fig. 4 FTIR spectra for chemical composition analysis of the fabricated 3D-printed scaffolds: **a** $SA/CH/GE_0$ (control); **b** pure gelatin powder (GE), $SA/CH/GE_5$, $SA/CH/GE_{10}$, and $SA/CH/GE_{15}$. FTIR: Fourier-transform infrared spectroscopy; SA: sodium alginate; CH: chitosan; GE: gelatin

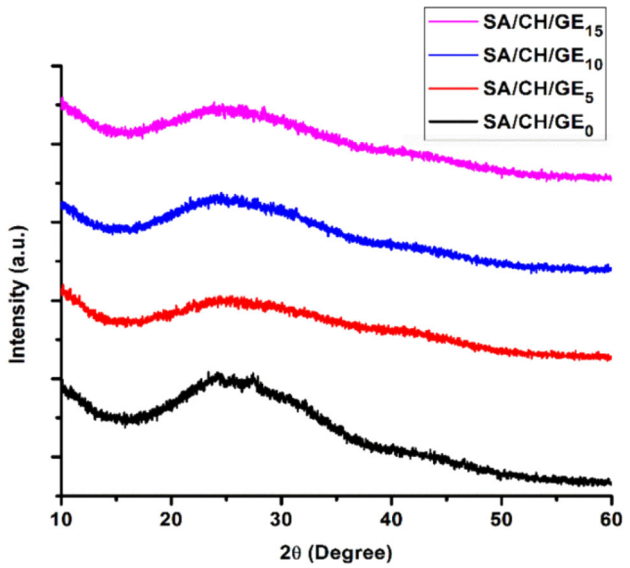

Fig. 5 XRD spectra of the 3D-printed SA/CH/GE scaffolds. XRD: X-ray diffraction; SA: sodium alginate; CH: chitosan; GE: gelatin

Hydrophilicity

The contact angle, which represents hydrophilicity, is an important surface property of a tissue scaffold. The hydrophilic surface of the scaffold promotes adsorption of proteins like vitronectin and fibronectin, as well as growth factors, thereby playing an important role in cell binding to the scaffold surface [90]. The contact angles measured for the SA/CH/GE scaffolds are displayed in Figs. 6a–6e. Gelatin film is reported to have a much higher contact angle than SA/CH-blend films [91–93], and hence the contact angles of the SA/CH blend films were enhanced with increasing amounts of gelatin. In comparison, the change in contact angle was not so significant among the SA/CH/GE scaffolds. However, a significant variation in the contact angle was observed between the $SA/CH/GE_{15}$ and control ($SA/CH/GE_0$) scaffolds. The highest contact angle (72.4°± 0.5°) was measured in the $SA/CH/GE_{15}$ scaffold. The composition of all the 3D-printed scaffolds showed contact angles far below θ=90°, confirming their hydrophilic nature [94]. Therefore, it can be hypothesized that the surface of scaffolds is favorable for the adherence of protein that may promote cell attachment thereby tissue regeneration [95].

Swelling behavior

Swelling is an important scaffold property for any tissue-engineering application. It is involved in the absorption of body fluid, diffusion of nutrients and growth factors to cells during in vitro cell study, and in in vivo implantation and removal of metabolic waste [71, 96–99]. The swelling of a scaffold should be controlled because extensive swelling may reduce the mechanical strength of the scaffold, besides causing rapid degradation [81]. Figure 6f displays the swelling pattern of the fabricated SA/CH/GE scaffolds. The maximum swelling was observed in the first two hours, followed by a gradual decline in fluid absorption until 8 h. No significant difference was observed in the swelling between 10 and 24 h in any of the scaffold compositions. The graph shows a declining swelling profile for the scaffolds with high gelatin content, because of relatively high hydrophilicity of

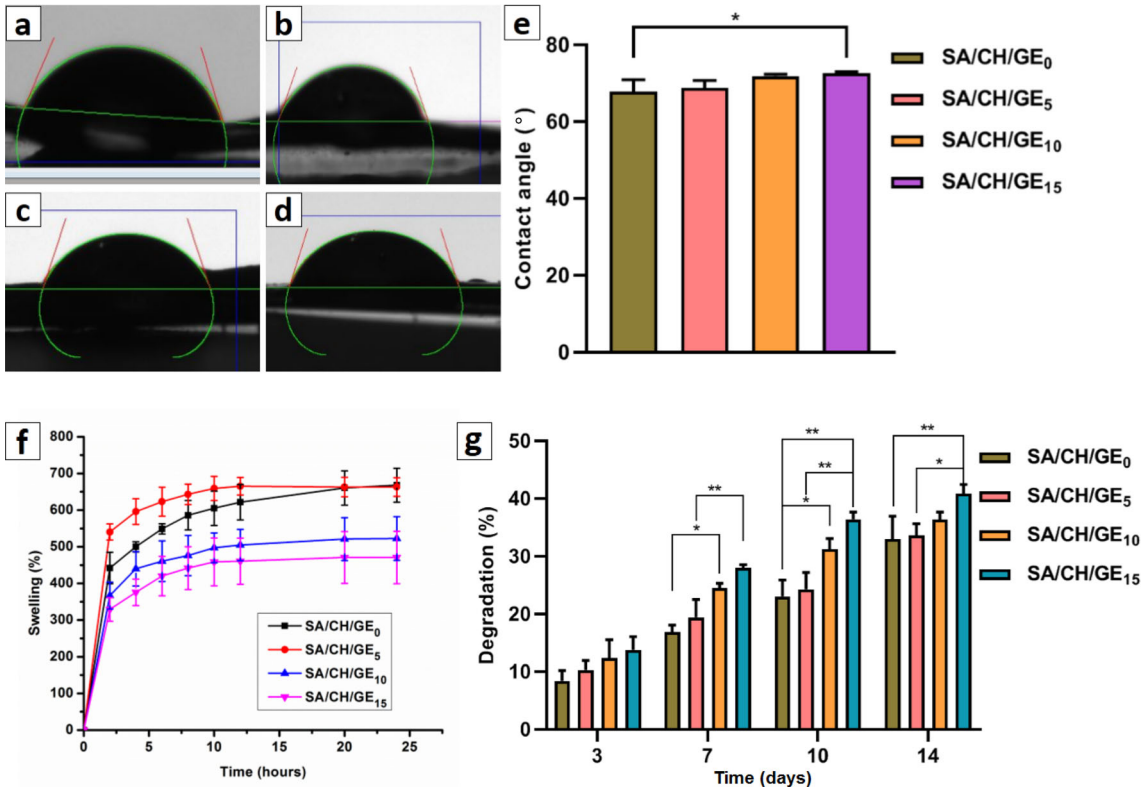

Fig. 6 Images showing the contact angles recorded using a drop shape analyzer for **a** SA/CH/GE_0 (control), **b** SA/CH/GE_5, **c** SA/CH/GE_{10}, and **d** SA/CH/GE_{15}; **e** measured contact angles of SA/CH/GE scaffolds; **f** swelling pattern of SA/CH/GE scaffolds; **g** degradation pattern of SA/CH/GE scaffolds. Data are presented as mean±standard deviation (n=3). $^{*}p<0.05$, $^{**}p\leq0.01$. SA: sodium alginate; CH: chitosan; GE: gelatin

the polyelectrolyte complex formed by the interaction of alginate, chitosan, and gelatin [100]. Another noteworthy explanation of the swelling behavior of SA/CH/GE scaffold is the crosslinking mechanism of gelatin with the EDC-NHS, which engages the free amines and carboxyl groups of the scaffold [99, 101].

During swelling, the fluid (SBF) is usually absorbed primarily in the pores and channels of the scaffold. When gelatin was added, we found that the overall solute content of the scaffold increased. Scaffolds with low polymeric solute content had more porous space to hold fluid, compared to scaffolds with a high polymeric concentration, which made them comparatively less porous [102]. The maximum swelling percentage of 667% was exhibited by SA/CH/GE_0, and the lowest by SA/CH/GE_{15}. This result can be correlated with the total solid polymeric content of the scaffold, which was higher in SA/CH/GE_{15} compared to the other scaffolds. The addition of gelatin decreased swelling, and this would be favorable for tissue engineering because high levels of swelling can reduce the stability and mechanical strength of the scaffold [81, 87].

Degradation study

Scaffolds for tissue engineering are designed to mimic the natural ECM, which allows cell attachment, proliferation, and differentiation during new tissue formation [87]. During this process, the scaffold gradually degrades, thereby providing space for new tissue to be formed. Ideally, the scaffold degradation rate should be equal to the rate of tissue-formation rate [103]. Therefore, assessing the degradation of scaffolds is vital. Figure 6g shows that degradation of the printed SA/CH/GE structures increased with longer exposure to SBF. Although the degradation was not significant till Day 3, a higher rate of degradation was shown by gelatin-containing scaffolds than the control scaffold. Afterward, the scaffold with high gelatin content degraded rapidly and we observed a significant difference between SA/CH/GE_0 and SA/CH/GE_{10} ($^{*}p<0.05$), as well as SA/CH/GE_5 and SA/CH/GE_{15} ($^{**}p\leq0.01$). The rapid degradation of scaffold containing gelatin may be attributable to fast hydrolyzation of gelatin due to the carboxylic and amine groups it contains

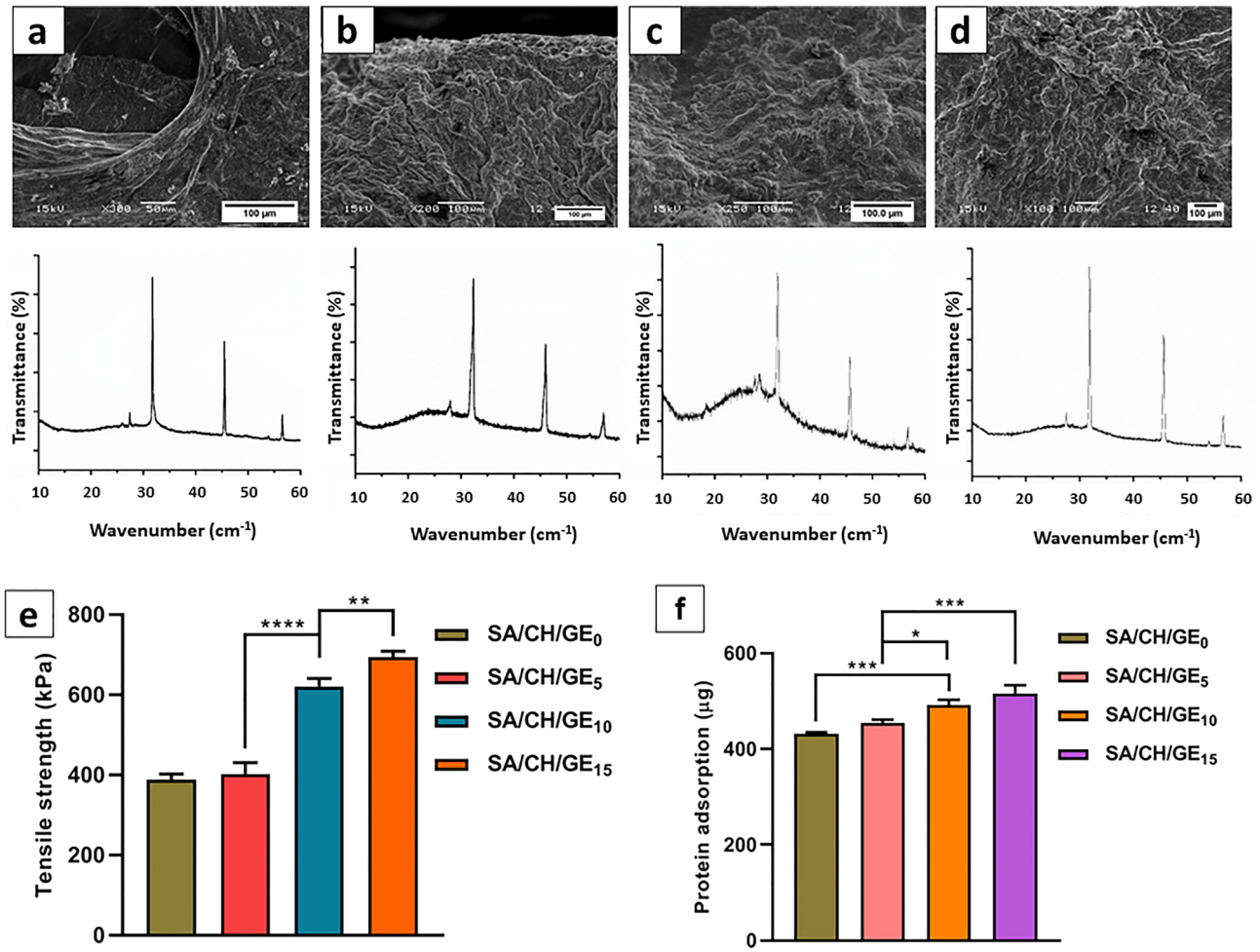

Fig. 7 SEM images and corresponding XRD patterns obtained by the biominerlization study with the fabricated scaffolds in SBF for 7d: **a** SA/CH/GE_0 (control), **b** SA/CH/GE_5, **c** SA/CH/GE_{10}, **d** SA/CH/GE_{15}, **e** measured tensile strength, and **f** protein adsorption of the 3D-printed SA/CH/GE scaffolds. Data are presented as mean±standard deviation (n=3). $^{*}p<0.05$, $^{**}p\leq0.01$, $^{***}p\leq0.001$, $^{****}p\leq0.0001$. SEM: scanning electron microscopy; XRD: X-ray diffraction; SBF: simulated body fluid; SA: sodium alginate; CH: chitosan; GE: gelatin

[101]. Of the various scaffolds, SA/CH/GE_{15} exhibited the greatest weight loss on Days 10 and 14. This behavior can be attributed to the sensitivity of the gelatin in aqueous solution, which results in rapid degradation of gelatin by hydrolization and formation of voids in place of gelatin in the bulk scaffold; this then leads to degradation of the entire SA/CH/GE scaffold [102].

In vitro bioactivity

In vitro bioactivity refers to the formation of a bone-like apatite layer over the scaffold surface. Bone-like apatite layers are deposited on the surface of the scaffold when it comes in contact with body fluid that helps in bonding with natural bone. This process is known as biomineralization and is a highly desirable one for scaffold used in bone-tissue regeneration [87, 104]. In this study, we analyzed the apatite layer deposited on the scaffold surface with SEM and XRD. The surface morphology of SA/CH/GE scaffolds is displayed in Figs. 7a–7d as it appeared after seven days of incubation. Apatite formation was exhibited by all the scaffold compositions. The SEM analysis revealed the high amount of mineral deposition over the scaffold with higher gelatin content. Gelatin has a bioinspired surface with carboxylate groups that easily bind to the calcium ions, thereby acting as nucleation points for apatite formation [105]. The XRD pattern of the scaffolds indicated peaks around 31.9°, 45.6°, and 56.6°, which were similar to the main characteristic peaks of hydroxyapatite (HAp) [106, 107]. The higher relative intensities represent a higher amount of apatite deposition, and thus it is evident that the best apatite deposition was obtained with SA/CH/GE_{15}. This result demonstrates the excellent bioactivity of the SA/CH/GE_{15} scaffold and hence its potential for bone-tissue regeneration.

Mechanical strength measurement

Mechanical strength is a crucial parameter which defines the mechanical integrity of a scaffold upon implantation in vivo and its survival during tissue regeneration. A scaffold should possess sufficient mechanical strength to provide structural stability under physiological conditions; it should offer mechanical support to the cells and newly formed tissue during in vitro as well as in vivo tissue formation [81]. The tensile strength of our scaffolds was in the range of (386 ±15)–(693±15) kPa; the higher value was obtained with higher gelatin content, as shown in Fig. 7e. The addition of gelatin to the SA/CH network significantly enhanced the tensile strength of the scaffolds. This is probably due to the stiff nature of the gelatin compared to sodium alginate and chitosan [101]. Therefore, blending gelatin with the SA/CH increased the overall stiffness of the fabricated scaffolds, which further improved the ultimate tensile strength. We found that the strength was directly related to the gelatin content of the scaffold. Similar results of enhancement in tensile strength of scaffold with incorporation of gelatin have been previously reported [85, 108, 109]. The maximum strength was shown by SA/CH/GE_{15}, compared to both the other scaffolds and the control.

Protein adsorption

The level of protein adsorption on the scaffold surface helps in determining the response of cells with the surface upon their interaction. Proteins like fibronectin and vitronectin are adsorbed on the surface of the scaffold when it comes in contact with body fluid, thereby facilitates the attachment, proliferation, and differentiation of cells over the scaffold surface [86, 87]. We calculated the protein adsorption for each SA/CH/GE scaffold composition; the adsorption patterns are shown in Fig. 7f. Protein adsorption increased upon the addition of gelatin, which may be attributed to the presence of more adsorption sites for protein over the scaffold surface; this is corroborated by an earlier report [102]. Gelatin, being the derivative of collagen, has the RGD sequence which encourages the protein adsorption that further facilitates cellular adhesion. Therefore, scaffolds with higher gelatin content have more RGD sequences that provide a higher number of protein-binding sites over the scaffold surface. So, we believe that, among the scaffolds fabricated in this study, the SA/CH/GE_{15} scaffold can provide the most favorable platform for cell attachment and proliferation.

MTT assay

We performed an MTT assay to investigate whether the 3D-printed scaffolds were cytocompatible . Saos-2 osteoblast-like cells were cultured over the scaffolds, and metabolic activity was monitored on Days 1, 3, and 5, as shown in Fig. 8. On the first day, we observed similar metabolic activity in all the 3D-printed scaffolds. However, as the culture progressed, cellular activity increased. We also noticed that the incorporated gelatin in the SA/CH scaffold network significantly enhanced the metabolic activity of cells. The highest cell metabolic activity was obtained with SA/CH/GE_{15}. This enhanced cell metabolic activity could be attributed to the availability of a higher number of cell-binding sites over the scaffold surface, due to the presence of the gelatin RGD sequence that promoted cell adhesion and proliferation [101, 110]. Thus, the developed 3D-printed SA/CH/GE scaffolds were demonstrated to be cytocompatible.

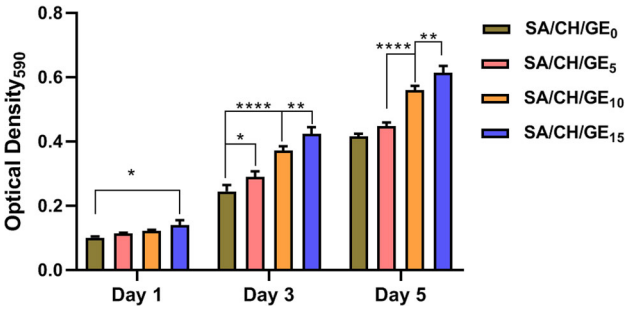

Fig. 8 MTT assay results obtained from the fabricated SA/CH/GE scaffolds at different time intervals during five days of Saos-2 cell culture. Data are presented as mean±standard deviation (n=3). $^{*}p<0.05$, $^{**}p\leq0.01$, $^{****}p\leq0.0001$.SA: sodium alginate; CH: chitosan; GE: gelatin

Cell attachment and cytoskeleton arrangement

The concept behind scaffolds is to provide a surface on which cells can attach and proliferate. When cells interact with the implanted scaffold, they attach, spread over the surface, and subsequently proliferate by cell division. Therefore, it was essential for us to inspect the newly developed scaffolds after cell seeding to confirm their compatibility with cellular growth. The morphology of the cells attached over the printed scaffolds was assessed by analyzing the SEM images captured on Day 4 and Day 7 of culture (Figs. 9a–9h). All four scaffold compositions showed well attachment of cells over their surfaces on the fourth day of culture. The cells had spread and proliferated on all the scaffolds on Day 7. These observations suggest that the SA/CH/GE scaffolds provided a favorable environment for cellular growth and were thus biocompatible. Moreover, the scaffolds containing gelatin showed better cell attachment and increased cell density in comparison to those without gelatin. SA/CH/GE scaffolds with higher gelatin content fostered enhanced cell density, probably because of the availability of more cell-binding

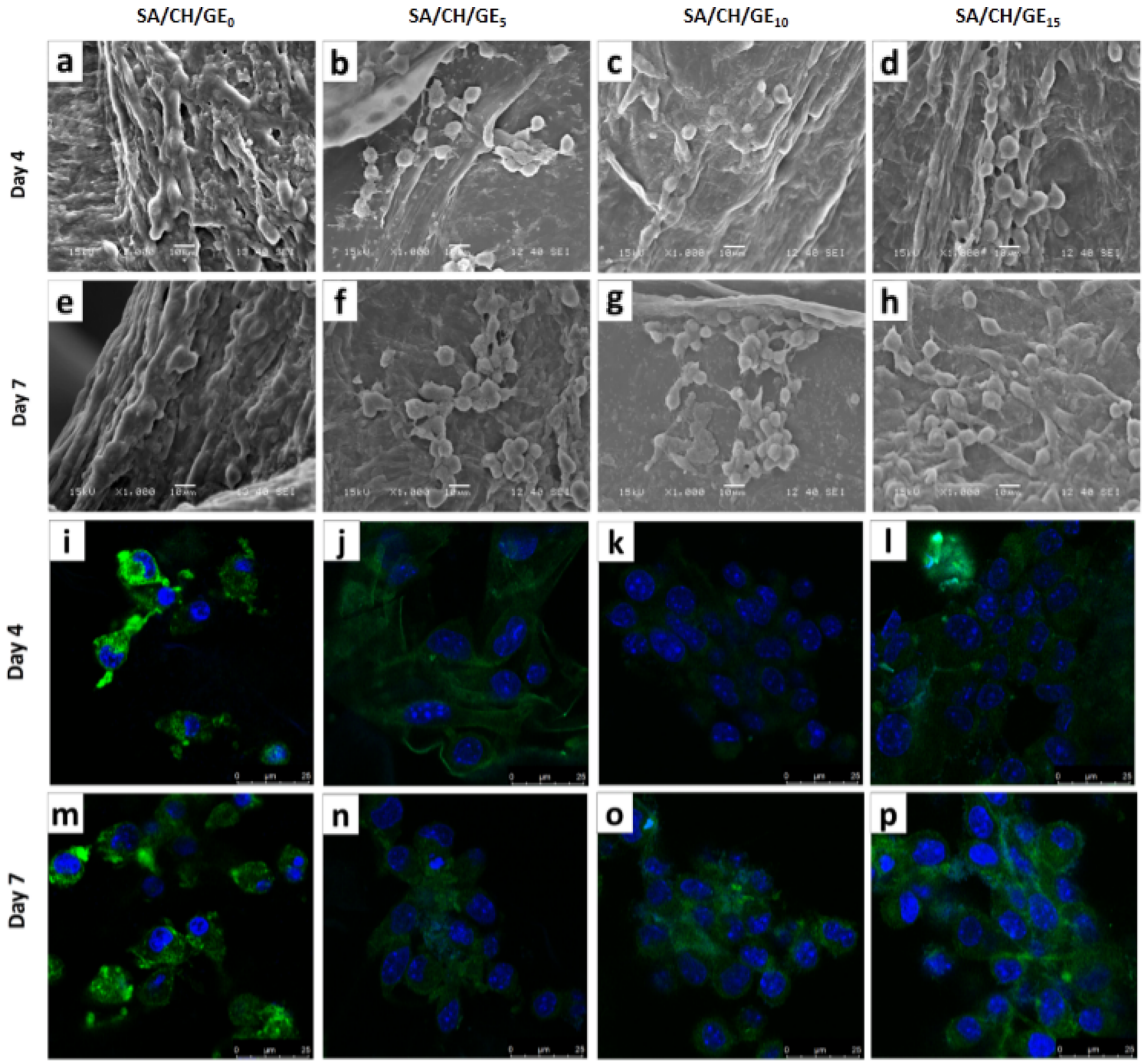

Fig. 9 SEM and confocal images for the assessment of cell attachment and cytoskeleton organization of cells cultured over the SA/CH/GE scaffolds, taken on Days 4 and 7. SEM images of the cells: $SA/CH/GE_0$ (**a**, **e**), $SA/CH/GE_5$ (**b**, **f**), $SA/CH/GE_{10}$ (**c**, **g**), and $SA/CH/GE_{15}$ (**d**, **h**). Confocal microscopic images of the cultured cells: $SA/CH/GE_0$ (**i**, **m**), $SA/CH/GE_5$ (**j**, **n**), $SA/CH/GE_{10}$ (**k**, **o**), and $SA/CH/GE_{15}$ (**l**, **p**). SEM: scanning electron microscopy; SA: sodium alginate; CH: chitosan; GE: gelatin

sites. Thus, they provided a more favorable microenvironment for cell attachment, migration, and proliferation [111].

We investigated cytoskeleton organization on the fourth and seventh days of cell culture by staining the actin filament with phalloidin and the nucleus with DAPI. The confocal microscope images of cytoskeleton organization are displayed in Figs. 9i–9p. The cells were found to be attached on the scaffold surface with low cell density on Day 4 of cell culture. However, the number of cells had increased, showing that the cells had proliferated well over the scaffold surface with the progression of the culture. On all the SA/CH/GE scaffolds, cells were found to have mixed morphology, including spherical and elongated shapes. However, more elongated cells were observed over the $SA/CH/GE_{15}$ scaffold compared to other scaffold compositions, indicating superior filamentous action. The density of cell attachment on the surface of the various scaffolds was improved by the addition of gelatin. Higher gelatin content led to higher cell proliferation, and accordingly, the highest cell density was obtained with the $SA/CH/GE_{15}$ scaffold. Thus, the fabrication of 3D-printed scaffolds that incorporate gelatin in the SA/CH scaffold network provides an enhanced cell-supportive surface which maintains the cytoskeleton organization of osteoblast-like cells that facilitates tissue regeneration.

In vitro biomineralization

ARS assay was performed to inspect biomineralization of the scaffolds by the cultured cells. ARS binds to the calcium

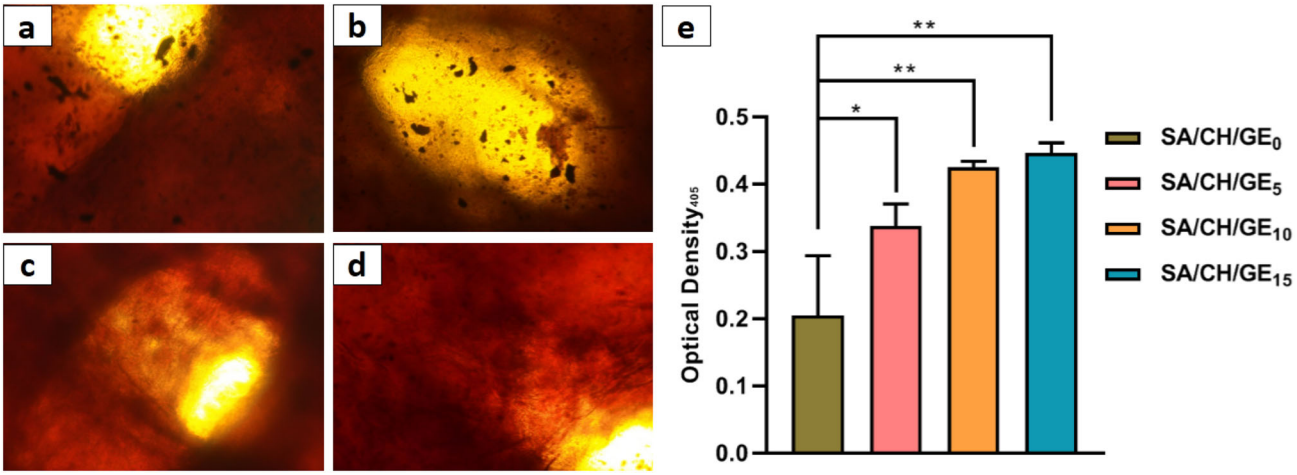

Fig. 10 Alizarin red S staining of the 3D-printed SA/CH/GE scaffolds: **a** SA/CH/GE_0 (control), **b** SA/CH/GE_5, **c** SA/CH/GE_{10}, and **d** SA/CH/GE_{15}; **e** quantitative analysis of the alizarin red S staining of the Saos-2 cells representing biomineralization activity on the scaffolds. Data are presented as mean±standard deviation (n=3). $^{*}p<0.05$, $^{**}p\leq0.01$. SA sodium alginate, CH chitosan, GE gelatin

produced by the osteoblast-like cells, forming an ARS–calcium complex [63]. The images and quantitative analysis of ARS-stained scaffolds are shown in Fig. 10. The images show dark red spots over all the scaffold surfaces, indicating the formation of mineralized inorganic matrix produced by the cells. This suggests that SA/CH/GE scaffold promotes biomineralization. However, the clearest and most prominent biomineralized nodules were found in SA/CH/GE_{10} and SA/CH/GE_{15}, indicating higher mineralization in scaffolds with higher gelatin content. Quantitative analysis of the ARS assay revealed that the addition of gelatin significantly enhanced biomineralization of the scaffolds, and that enhanced biomineralization modules were formed with increased content of gelatin in the scaffolds. The higher ECM biomineralization obtained with SA/CH/GE_{15} indicated higher cell proliferation in comparison to the other scaffold compositions [105]. We therefore concluded that gelatin-containing SA/CH scaffold might be a suitable platform for cell adhesion, proliferation, and differentiation to promote bone regeneration.

Conclusions

In this study, we developed sodium alginate/chitosan/gelatin tri-polymeric complexes with different compositions as bioinks for 3D printing, allowing us to fabricate SA/CH/GE scaffold structures with varying gelatin content (0%–15%, volume fraction). These 3D-printed scaffolds were designated as SA/CH/GE_0 (control), SA/CH/GE_5, SA/CH/GE_{10}, and SA/CH/GE_{15}. SEM images displayed the layer-by-layer 3D assembly of the microfibrous scaffold structures, which had interconnected porous networks and the desired pore-size range. All the scaffold compositions exhibited acceptable contact angles (<90°) reflecting their hydrophilic nature, degradation with a trend of SA/CH/GE_0<SA/CH/GE_5<SA/CH/GE_{10}<SA/CH/GE_{15}, and swelling. The most controlled swelling behavior was seen in scaffolds with higher gelatin content. The in vitro biomineralization determined by ARS assay and protein-adsorption studies revealed higher bioactivity and cell adhesion properties in scaffolds containing gelatin, confirming these scaffolds as suitable template for BTE. The cell-supportive properties of all the fabricated SA/CH/GE structures are evident from the in vitro cell studies. The scaffolds promote cell attachment, viability, and proliferation, which further augments biomineralization (forming an apatite layer over the surface). Therefore, it has been demonstrated here that the incorporation of gelatin in SA/CH scaffold makes it a potential substrate for BTE. Furthermore, SA/CH/GE with 15% gelatin content (SA/CH/GE_{15}) is the most suitable among all the printed scaffold compositions we tested.

Acknowledgements The authors are thankful to Ministry of Human Resource Development (presently Ministry of Education), Government of India, New Delhi, for providing research facility by sanctioning Center of Excellence (F. No. 5-6/2013- TS VII) in Tissue Engineering and Center of Excellence in Orthopedic Tissue Engineering and Rehabilitation funded by World Bank under TEQIP-II.

Author contributions AKS contributed to investigation, methodology, conceptualization, and writing. KP contributed to resources, supervision, conceptualization, and writing—review and editing. AB contributed to review and editing.

Declarations

Conflict of interest The authors declare that they have no known competing financial interests or personal relationships that could have appeared to influence the work reported in this paper.

Ethical approval This article does not contain any studies with human or animal subjects performed by any of the authors.

References

1. Singh AK, Pramanik K, Biswas A (2019) MgO enables enhanced bioactivity and antimicrobial activity of nano bioglass for bone tissue engineering application. Mater Technol 34(13):818–826. https://doi.org/10.1080/10667857.2019.1638636
2. Zhang WC, Ullah I, Shi L et al (2019) Fabrication and characterization of porous polycaprolactone scaffold via extrusion-based cryogenic 3D printing for tissue engineering. Mater Des 180:107946. https://doi.org/10.1016/j.matdes.2019.107946
3. Singh YP, Bhaskar R, Agrawal AK et al (2022) Effect of monetite reinforced into the chitosan-based lyophilized 3D scaffolds on physicochemical, mechanical, and osteogenic properties. Int J Polym Mater Polym Biomater. https://doi.org/10.1080/00914037.2022.2090358
4. Singh YP, Dasgupta S, Bhaskar R (2019) Preparation, characterization and bioactivities of nano anhydrous calcium phosphate added gelatin–chitosan scaffolds for bone tissue engineering. J Biomater Sci Polym Ed 30(18):1756–1778. https://doi.org/10.1080/09205063.2019.1663474
5. Ergul NM, Unal S, Kartal I et al (2019) 3D printing of chitosan/poly (vinyl alcohol) hydrogel containing synthesized hydroxyapatite scaffolds for hard-tissue engineering. Polym Test 79:106006. https://doi.org/10.1016/j.polymertesting.2019.106006
6. Croisier F, Jérôme C (2013) Chitosan-based biomaterials for tissue engineering. Eur Polym J 49(4):780–792. https://doi.org/10.1016/j.eurpolymj.2012.12.009
7. Singh YP, Mishra B, Gupta MK et al (2023) Gelatin/monetite electrospun scaffolds to regenerate bone tissue: fabrication, characterization, and in-vitro evaluation. J Mech Behav Biomed Mater 137:105524. https://doi.org/10.1016/j.jmbbm.2022.105524
8. Singh YP, Dasgupta S, Nayar S et al (2020) Optimization of electrospinning process & parameters for producing defect-free chitosan/polyethylene oxide nanofibers for bone tissue engineering. J Biomater Sci Polym Ed 31(6):781–803. https://doi.org/10.1080/09205063.2020.1718824
9. Purohit SD, Singh H, Bhaskar R et al (2020) Gelatin—alginate—cerium oxide nanocomposite scaffold for bone regeneration. Mater Sci Eng C 116:111111. https://doi.org/10.1016/j.msec.2020.111111
10. Singh YP, Dasgupta S, Bhaskar R et al (2021) Monetite addition into gelatin based freeze-dried scaffolds for improved mechanical and osteogenic properties. Biomed Mater 16:065030. https://doi.org/10.1088/1748-605X/ac2e17
11. Bhattacharjee P, Kundu B, Naskar D et al (2017) Silk scaffolds in bone tissue engineering: an overview. Acta Biomater 63:1–17. https://doi.org/10.1016/j.actbio.2017.09.027
12. Sánchez-Salcedo S, Nieto A, Vallet-Regí M (2018) Hydroxyapatite/β-tricalcium phosphate/agarose macroporous scaffolds for bone tissue engineering. Chem Eng J 137(1):62–71. https://doi.org/10.1016/j.cej.2007.09.011
13. Verma N, Pramanik K, Singh AK et al (2022) Design of magnesium oxide nanoparticle incorporated carboxy methyl cellulose/poly vinyl alcohol composite film with novel composition for skin tissue engineering. Mater Tech 37(8):706–716. https://doi.org/10.1080/10667857.2021.1873634
14. Gautam S, Sharma C, Purohit SD et al (2021) Gelatin-polycaprolactone-nanohydroxyapatite electrospun nanocomposite scaffold for bone tissue engineering. Mater Sci Eng C 119:111588. https://doi.org/10.1016/j.msec.2020.111588
15. Pushp P, Bhaskar R, Kelkar S et al (2021) Plasticized poly(vinylalcohol) and poly(vinylpyrrolidone) based patches with tunable mechanical properties for cardiac tissue engineering applications. Biotech Bioeng 118(6):2312–2325. https://doi.org/10.1002/bit.27743
16. Sreekumaran S, Radhakrishnan A, Rauf AA et al (2021) Nanohydroxyapatite incorporated photocrosslinked gelatin methacryloyl/poly(ethylene glycol) diacrylate hydrogel for bone tissue engineering. Prog Biomater 10(1):43–51. https://doi.org/10.1007/s40204-021-00150-x
17. Coimbra P, Ferreira P, de Sousa HC et al (2011) Preparation and chemical and biological characterization of a pectin/chitosan polyelectrolyte complex scaffold for possible bone tissue engineering applications. Int J Biol Macromol 48(1):112–118. https://doi.org/10.1016/j.ijbiomac.2010.10.006
18. Wang YY, Wang XY, Shi J et al (2016) A biomimetic silk fibroin/sodium alginate composite scaffold for soft tissue engineering. Sci Rep 6:39477. https://doi.org/10.1038/srep39477
19. Wu JW, Miao GH, Zheng ZC et al (2019) 3D printing mesoporous bioactive glass/sodium alginate/gelatin sustained release scaffolds for bone repair. J Biomater Appl 33(6):755–765. https://doi.org/10.1177/0885328218810269
20. Bi YG, Lin ZT, Deng ST (2019) Fabrication and characterization of hydroxyapatite/sodium alginate/chitosan composite microspheres for drug delivery and bone tissue engineering. Mater Sci Eng C 100:576–583. https://doi.org/10.1016/j.msec.2019.03.040
21. Zheng A, Cao LY, Liu Y et al (2018) Biocompatible silk/calcium silicate/sodium alginate composite scaffolds for bone tissue engineering. Carbohydr Polym 199(1):244–255. https://doi.org/10.1016/j.carbpol.2018.06.093
22. Venkatesan J, Bhatnagar I, Manivasagan P et al (2015) Alginate composites for bone tissue engineering: a review. Int J Biol Macromol 72:269–281. https://doi.org/10.1016/j.ijbiomac.2014.07.008
23. Saravanakumar K, Sathiyaseelan A, Mariadoss AVA et al (2020) Physical and bioactivities of biopolymeric films incorporated with cellulose, sodium alginate and copper oxide nanoparticles for food packaging application. Int J Biol Macromol 153:207–214. https://doi.org/10.1016/j.ijbiomac.2020.02.250
24. Zhao J, Zhu YW, He GW et al (2016) Incorporating zwitterionic graphene oxides into sodium alginate membrane for efficient water/alcohol separation. ACS Appl Mater Interfaces 8(3):2097–2103. https://doi.org/10.1021/acsami.5b10551
25. Fan LH, Ge HY, Zou SQ et al (2016) Sodium alginate conjugated graphene oxide as a new carrier for drug delivery system. Int J Biol Macromol 93:582–590. https://doi.org/10.1016/j.ijbiomac.2016.09.026
26. Solovieva EV, Fedotov AY, Mamonov VE et al (2018) Fibrinogen-modified sodium alginate as a scaffold material for skin tissue engineering. Biomed Mater 13(2):025007. https://doi.org/10.1088/1748-605X/aa9089
27. Wu ZX, Li Q, Xie S et al (2020) In vitro and in vivo biocompatibility evaluation of a 3D bioprinted gelatin-sodium alginate/rat Schwann-cell scaffold. Mater Sci Eng C 109:110530. https://doi.org/10.1016/j.msec.2019.110530
28. Bastiaens L, Soetemans L, D'Hondt E et al (2019) Sources of chitin and chitosan and their isolation. In: van den Broek LAM, Boeriu CG, Stevens CV (Eds.), Chitin and Chitosan: Properties Applications. Wiley, p.1–34. https://doi.org/10.1002/9781119450467

29. Oryan A, Sahvieh S (2017) Effectiveness of chitosan scaffold in skin, bone and cartilage healing. Int J Biol Macromol 104:1003–1011. https://doi.org/10.1016/j.ijbiomac.2017.06.124
30. LogithKumar R, KeshavNarayan A, Dhivya S et al (2016) A review of chitosan and its derivatives in bone tissue engineering. Carbohydr Polym 151:172–188. https://doi.org/10.1016/j.carbpol.2016.05.049
31. Ahmed S, Ali A, Sheikh J (2018) A review on chitosan centred scaffolds and their applications in tissue engineering. Int J Biol Macromol 116:849–862. https://doi.org/10.1016/j.ijbiomac.2018.04.176
32. Baranwal A, Kumar A, Priyadharshini A et al (2018) Chitosan: an undisputed bio-fabrication material for tissue engineering and biosensing applications. Int J Biol Macromol 110:110–123. https://doi.org/10.1016/j.ijbiomac.2018.01.006
33. Gümüşderelioğlu M, Aday S (2011) Heparin-functionalized chitosan scaffolds for bone tissue engineering. Carbohydr Res 346(5):606–613. https://doi.org/10.1016/j.carres.2010.12.007
34. Sharma C, Dinda AK, Potdar PD et al (2016) Fabrication and characterization of novel nano-biocomposite scaffold of chitosan–gelatin–alginate–hydroxyapatite for bone tissue engineering. Mater Sci Eng C 64:416–427. https://doi.org/10.1016/j.msec.2016.03.060
35. Narayanan KB, Bhaskar R, Han SS (2022) Recent advances in the biomedical applications of functionalized nanogels. Pharmaceutics 14(12):2832. https://doi.org/10.3390/pharmaceutics14122832
36. Saekhor K, Udomsinprasert W, Honsawek S et al (2019) Preparation of an injectable modified chitosan-based hydrogel approaching for bone tissue engineering. Int J Biol Macromol 123:167–173. https://doi.org/10.1016/j.ijbiomac.2018.11.041
37. Li Q, Lu F, Zhou GF et al (2017) Silver inlaid with gold nanoparticle/chitosan wound dressing enhances antibacterial activity and porosity, and promotes wound healing. Biomacromol 18(11):3766–3775. https://doi.org/10.1021/acs.biomac.7b01180
38. Kim CH, Park SJ, Yang DH et al (2018) Chitosan for tissue engineering. In: Chun HJ, Park K, Kim CH et al (Eds.), Novel Biomaterials for Regenerative Medicine. Springer, Singapore, p.475–485. https://doi.org/10.1007/978-981-13-0947-2
39. Prakash J, Prema D, Venkataprasanna KS et al (2020) Nanocomposite chitosan film containing graphene oxide/hydroxyapatite/gold for bone tissue engineering. Int J Biol Macromol 154:62–71. https://doi.org/10.1016/j.ijbiomac.2020.03.095
40. de Souza FCB, de Souza RFB, Drouin B et al (2019) Comparative study on complexes formed by chitosan and different polyanions: potential of chitosan-pectin biomaterials as scaffolds in tissue engineering. Int J Biol Macromol 132:178–189. https://doi.org/10.1016/j.ijbiomac.2019.03.187
41. Kim HL, Jung GY, Yoon JH et al (2015) Preparation and characterization of nano-sized hydroxyapatite/alginate/chitosan composite scaffolds for bone tissue engineering. Mater Sci Eng C 54:20–25. https://doi.org/10.1016/j.msec.2015.04.033
42. Alsharabasy AM, Moghannem SA, El-Mazny WN et al (2015) Physical preparation of alginate/chitosan polyelectrolyte complexes for biomedical applications. J Biomater Appl 30(7):1071–1079. https://doi.org/10.1177/0885328215613886
43. Singh AK, Pramanik K (2023) Fabrication and investigation of physicochemical and biological properties of 3D printed sodium alginate-chitosan blend polyelectrolyte complex scaffold for bone tissue engineering application. J Appl Polymer Sci 140(12):18. https://doi.org/10.1002/app.53642
44. Chong EJ, Phan TT, Lim IJ et al (2007) Evaluation of electrospun PCL/gelatin nanofibrous scaffold for wound healing and layered dermal reconstitution. Acta Biomater 3(3):321–330. https://doi.org/10.1016/j.actbio.2007.01.002
45. Lien SM, Ko LY, Huang TJ (2008) Effect of pore size on ECM secretion and cell growth in gelatin scaffold for articular cartilage tissue engineering. Acta Biomater 5(2):670–679. https://doi.org/10.1016/j.actbio.2008.09.020
46. Peter M, Binulal N, Nair S et al (2010) Novel biodegradable chitosan–gelatin/nano-bioactive glass ceramic composite scaffolds for alveolar bone tissue engineering. Chem Eng J 158(2):353–361. https://doi.org/10.1016/j.cej.2010.02.003
47. Purohit SD, Singh H, Bhaskar R et al (2020) Fabrication of graphene oxide and nanohydroxyapatite reinforced gelatin–alginate nanocomposite scaffold for bone tissue regeneration. Front Mater 7:250. https://doi.org/10.3389/fmats.2020.00250
48. Hoque ME, Nuge T, Yeow TK et al (2015) Gelatin based scaffolds for tissue engineering—a review. Polym Res J 9(1):15
49. Sakthiguru N, Sithique MA (2020) Fabrication of bioinspired chitosan/gelatin/allantoin biocomposite film for wound dressing application. Int J Biol Macromol 152:873–883. https://doi.org/10.1016/j.ijbiomac.2020.02.289
50. Pan T, Song WJ, Cao XD et al (2016) 3D bioplotting of gelatin/alginate scaffolds for tissue engineering: influence of crosslinking degree and pore architecture on physicochemical properties. J Mater Sci Tech 32(9):889–900. https://doi.org/10.1016/j.jmst.2016.01.007
51. Zarif ME (2018) A review of chitosan-, alginate-, and gelatin-based biocomposites for bone tissue engineering. Biomater Tissue Eng Bull 5(3–4):97–109. https://doi.org/10.33263/BTEB534.097109
52. Levengood SKL, Zhang MQ (2014) Chitosan-based scaffolds for bone tissue engineering. J Mater Chem B 2(21):3161–3184. https://doi.org/10.1039/c4tb00027g
53. Ranganathan S, Balagangadharan K, Selvamurugan N (2019) Chitosan and gelatin-based electrospun fibers for bone tissue engineering. Int J Biol Macromol 133:354–364. https://doi.org/10.1016/j.ijbiomac.2019.04.115
54. Gautam S, Dinda AK, Mishra NC (2013) Fabrication and characterization of PCL/gelatin composite nanofibrous scaffold for tissue engineering applications by electrospinning method. Mater Sci Eng C 33:1228–1235. https://doi.org/10.1016/j.msec.2012.12.015
55. Haleem A, Javaid M, Khan RH et al (2020) 3D printing applications in bone tissue engineering. J Clin Orthop Trauma 11:S118–S124. https://doi.org/10.1016/j.jcot.2019.12.002
56. Wang HQ, Cui JY, Li ST et al (2022) Fabrication of functional and biodegradable scaffolds using nucleated poly(4-hydroxybutyrate) via 3D printing for bone tissue engineering. Polym Test 118:107881. https://doi.org/10.1016/j.polymertesting.2022.107881
57. Leukers B, Gülkan H, Irsen SH et al (2005) Hydroxyapatite scaffolds for bone tissue engineering made by 3D printing. J Mater Sci Mater Med 16(12):1121–1124. https://doi.org/10.1007/s10856-005-4716-5
58. Singh B, Panda N, Pramanik K (2016) A novel electrospinning approach to fabricate high strength aqueous silk fibroin nanofibers. Int J Biol Macromol 87:201–207. https://doi.org/10.1016/j.ijbiomac.2016.01.120
59. Agrawal P, Pramanik K (2016) Chitosan-poly(vinyl alcohol) nanofibers by free surface electrospinning for tissue engineering applications. Tissue Eng Regener Med 13:485–497. https://doi.org/10.1007/s13770-016-9092-3
60. Martínez-Vázquez F, Cabañas M, Paris J et al (2015) Fabrication of novel Si-doped hydroxyapatite/gelatine scaffolds by rapid prototyping for drug delivery and bone regeneration. Acta Biomater 15:200–209. https://doi.org/10.1016/j.actbio.2014.12.021

61. Kokubo T, Kim HM, Kawashita M (2003) Novel bioactive materials with different mechanical properties. Biomaterials 24(13):2161–2175. https://doi.org/10.1016/S0142-9612(03)00044-9
62. Asadi N, Alizadeh E, Del Bakhshayesh AR et al (2019) Fabrication and in vitro evaluation of nanocomposite hydrogel scaffolds based on gelatin/PCL–PEG–PCL for cartilage tissue engineering. ACS Omega 4(1):449–457. https://doi.org/10.1021/acsomega.8b02593
63. Singh B, Panda N, Mund R et al (2016) Carboxymethyl cellulose enables silk fibroin nanofibrous scaffold with enhanced biomimetic potential for bone tissue engineering application. Carbohydr Polym 151:335–347. https://doi.org/10.1016/j.carbpol.2016.05.088
64. Dixit K, Kulanthaivel S, Agarwal T et al (2022) Gum tragacanth modified nano-hydroxyapatite: an angiogenic-osteogenic biomaterial for bone tissue engineering. Ceram Int 48(10):14672–14683. https://doi.org/10.1016/j.ceramint.2022.02.002
65. Singh BN, Pramanik K (2017) Development of novel silk fibroin/polyvinyl alcohol/sol–gel bioactive glass composite matrix by modified layer by layer electrospinning method for bone tissue construct generation. Biofabrication 9:015028. https://doi.org/10.1088/1758-5090/aa644f
66. Feroz S, Dias G (2021) Hydroxypropylmethyl cellulose (HPMC) crosslinked keratin/hydroxyapatite (HA) scaffold fabrication, characterization and in vitro biocompatibility assessment as a bone graft for alveolar bone regeneration. Heliyon 7(11):e08294. https://doi.org/10.1016/j.heliyon.2021.e08294
67. Cui N, Qian J, Liu T et al (2015) Hyaluronic acid hydrogel scaffolds with a triple degradation behavior for bone tissue engineering. Carbohydr Polym 126:192–198. https://doi.org/10.1016/j.carbpol.2015.03.013
68. Mallick SP, Singh BN, Rastogi A et al (2018) Design and evaluation of chitosan/poly(L-lactide)/pectin based composite scaffolds for cartilage tissue regeneration. Int J Biol Macromol 112:909–920. https://doi.org/10.1016/j.ijbiomac.2018.02.049
69. Kundu K, Afshar A, Katti DR et al (2021) Composite nanoclay-hydroxyapatite-polymer fiber scaffolds for bone tissue engineering manufactured using pressurized gyration. Compos Sci Tech 202:108598. https://doi.org/10.1016/j.compscitech.2020.108598
70. Agrawal P, Pramanik K, Biswas A (2018) Chondrogenic differentiation of mesenchymal stem cells on silk fibroin: chitosan–glucosamine scaffold in dynamic culture. Regener Med 13:545–558. https://doi.org/10.2217/rme-2017-0159
71. Peter M, Ganesh N, Selvamurugan N et al (2010) Preparation and characterization of chitosan–gelatin/nanohydroxyapatite composite scaffolds for tissue engineering applications. Carbohydr Polym 80:687–694. https://doi.org/10.1016/j.carbpol.2020.116899
72. Gautam S, Purohit SD, Singh H et al (2023) Surface modification of PCL-gelatin-chitosan electrospun scaffold by nano-hydroxyapatite for bone tissue engineering. Mater Today Commun 34:105237. https://doi.org/10.1016/j.mtcomm.2022.105237
73. Jodati H, Evis Z, Tezcaner A et al (2023) 3D porous bioceramic based boron-doped hydroxyapatite/baghdadite composite scaffolds for bone tissue engineering. J Mech Behav Biomed Mater 140:105722. https://doi.org/10.1016/j.jmbbm.2023.105722
74. Liu QQ, Li QT, Xu S et al (2018) Preparation and properties of 3D printed alginate–chitosan polyion complex hydrogels for tissue engineering. Polymers 10(6):664. https://doi.org/10.3390/polym10060664
75. Jiang YN, Zhou JP, Feng C et al (2020) Rheological behavior, 3D printability and the formation of scaffolds with cellulose nanocrystals/gelatin hydrogels. J Mater Sci 55(33):15709–15725. https://doi.org/10.1007/s10853-020-05128-x
76. Habib A, Sathish V, Mallik S et al (2018) 3D printability of alginate-carboxymethyl cellulose hydrogel. Materials 11(3):454. https://doi.org/10.3390/ma11030454
77. Chen JF, Garcia ES, Zimmerman SC (2020) Intramolecularly cross-linked polymers: from structure to function with applications as artificial antibodies and artificial enzymes. Acc Chem Res 53(6):1244–1256. https://doi.org/10.1021/acs.accounts.0c00178
78. Fertah M, Belfkira A, Taourirte M et al (2017) Extraction and characterization of sodium alginate from Moroccan *Laminaria digitata* brown seaweed. Arab J Chem 10(S2):S3707–S3714. https://doi.org/10.1016/j.arabjc.2014.05.003
79. Narra K, Dhanalekshmi U, Rangaraj G et al (2012) Effect of formulation variables on rifampicin loaded alginate beads. IJPR 11(3):715–721. https://doi.org/10.1016/0378-5173(94)00238-Z
80. Li ZS, Ramay HR, Hauch KD et al (2005) Chitosan–alginate hybrid scaffolds for bone tissue engineering. Biomaterials 26(18):3919–3928. https://doi.org/10.1016/j.biomaterials.2004.09.062
81. Li T, Liu ZL, Xiao M et al (2017) In vitro and in vivo studies of a gelatin/carboxymethyl chitosan/LAPONITE® composite scaffold for bone tissue engineering. RSC Adv 7(85):54100–54110. https://doi.org/10.1039/c7ra06913h
82. Sharma C, Dinda AK, Mishra NC (2013) Fabrication and characterization of natural origin chitosan-gelatin-alginate composite scaffold by foaming method without using surfactant. J Appl Polym Sci 127(4):3228–3241. https://doi.org/10.1002/app.37755
83. Yan HQ, Chen XQ, Feng MX et al (2017) Layer-by-layer assembly of 3D alginate-chitosan-gelatin composite scaffold incorporating bacterial cellulose nanocrystals for bone tissue engineering. Mater Lett 209:492–496. https://doi.org/10.1016/j.matlet.2017.08.093
84. Dong ZH, Li YB, Zou Q (2009) Degradation and biocompatibility of porous nano-hydroxyapatite/polyurethane composite scaffold for bone tissue engineering. Appl Surf Sci 255(12):6087–6091. https://doi.org/10.1016/j.apsusc.2009.01.083
85. Badhe RV, Bijukumar D, Chejara DR et al (2017) A composite chitosan-gelatin bi-layered, biomimetic macroporous scaffold for blood vessel tissue engineering. Carbohydr Polym 157:1215–1225. https://doi.org/10.1016/j.carbpol.2016.09.095
86. Venkatesan J, Bhatnagar I, Kim SK (2014) Chitosan-alginate biocomposite containing fucoidan for bone tissue engineering. Mar Drugs 12(1):300–316. https://doi.org/10.3390/md12010300
87. Nga NK, Tam LTT, Ha NT et al (2020) Enhanced biomineralization and protein adsorption capacity of 3D chitosan/hydroxyapatite biomimetic scaffolds applied for bone-tissue engineering. RSC Adv 1(7):4345–4357. https://doi.org/10.1039/d0ra09432c
88. Castel-Molieres M, Conzatti G, Torrisani J et al (2018) Influence of homogenization technique and blend ratio on chitosan/alginate polyelectrolyte complex properties. J Med Biol Eng 38(1):10–21. https://doi.org/10.1007/s40846-017-0304-7
89. Mathews S, Gupta PK, Bhonde R et al (2011) Chitosan enhances mineralization during osteoblast differentiation of human bone marrow-derived mesenchymal stem cells, by upregulating the associated genes. Cell Prolif 44(6):537–549. https://doi.org/10.1111/j.1365-2184.2011.00788.x
90. Zhang J, Li JN, Jia GL et al (2017) Improving osteogenesis of PLGA/HA porous scaffolds based on dual delivery of BMP-2 and IGF-1 via a polydopamine coating. RSC Adv 7(89):56732–56742. https://doi.org/10.1039/c7ra12062a
91. Lavrič G, Oberlintner A, Filipova I et al (2021) Functional nanocellulose, alginate and chitosan nanocomposites designed as active film packaging materials. Polymers 13(15):2523. https://doi.org/10.3390/polym13152523
92. Pereira RF, Carvalho A, Gil MH et al (2013) Influence of *Aloe vera* on water absorption and enzymatic in vitro degradation of

alginate hydrogel films. Carbohydr Polym 98(1):311–320. https://doi.org/10.1016/j.carbpol.2013.05.076
93. Li K, Jin SC, Chen H et al (2019) Bioinspired interface engineering of gelatin/cellulose nanofibrils nanocomposites with high mechanical performance and antibacterial properties for active packaging. Compos Part B Eng 171:222–234. https://doi.org/10.1016/j.compositesb.2019.04.043
94. Huang A, Jiang YC, Napiwocki B et al (2017) Fabrication of poly(ε-caprolactone) tissue engineering scaffolds with fibrillated and interconnected pores utilizing microcellular injection molding and polymer leaching. RSC Adv 7(69):43432–43444. https://doi.org/10.1039/c7ra06987a
95. Liu Y, Xu CL, Gu Y et al (2019) Polydopamine-modified poly(L-lactic acid) nanofiber scaffolds immobilized with an osteogenic growth peptide for bone tissue regeneration. RSC Adv 9(21):11722–11736. https://doi.org/10.1039/c8ra08828d
96. Singh D, Tripathi A, Zo S et al (2014) Synthesis of composite gelatin-hyaluronic acid-alginate porous scaffold and evaluation for in vitro stem cell growth and in vivo tissue integration. Colloids Surf B Biointerfaces 116:502–509. https://doi.org/10.1016/j.colsurfb.2014.01.049
97. Alven S, Khwaza V, Oyedeji OO et al (2021) Polymer-based scaffolds loaded with *Aloe vera* extract for the treatment of wounds. Pharmaceutics 13(7):961. https://doi.org/10.3390/pharmaceutics13070961
98. Aghmiuni AI, Keshel SH, Sefat F et al (2021) Fabrication of 3D hybrid scaffold by combination technique of electrospinning-like and freeze-drying to create mechanotransduction signals and mimic extracellular matrix function of skin. Mater Sci Eng C 120:111752. https://doi.org/10.1016/j.msec.2020.111752
99. Li JJ, Sun H, Sun D et al (2011) Biomimetic multicomponent polysaccharide/nano-hydroxyapatite composites for bone tissue engineering. Carbohydr Polym 85(4):885–894. https://doi.org/10.1016/j.carbpol.2011.04.015
100. Chen Y, Duan QF, Yu L et al (2021) Thermomechanically processed chitosan: gelatin films being transparent, mechanically robust and less hygroscopic. Carbohydr Polym 272:118522. https://doi.org/10.1016/j.carbpol.2021.118522
101. Afjoul H, Shamloo A, Kamali A (2020) Freeze-gelled alginate/gelatin scaffolds for wound healing applications: an in vitro, in vivo study. Mater Sci Eng C 113:110957. https://doi.org/10.1016/j.msec.2020.110957
102. Nieto-Suárez M, López-Quintela MA, Lazzari M (2016) Preparation and characterization of crosslinked chitosan/gelatin scaffolds by ice segregation induced self-assembly. Carbohydr Polym 141:175–183. https://doi.org/10.1016/j.carbpol.2015.12.064
103. Begum E, Rajaiah S, Bhavani K et al (2017) Evaluation of extracted chitosan from Portunus pelagicus for the preparation of chitosan alginate blend scaffolds. J Polym Environ 25(3):578–585. https://doi.org/10.1007/s10924-016-0834-z
104. Luo HL, Zhang Y, Li G et al (2017) Sacrificial template method for the synthesis of three-dimensional nanofibrous 58S bioglass scaffold and its in vitro bioactivity and cell responses. J Biomater Appl 32(2):265–275. https://doi.org/10.1177/0885328217715784
105. Liu HY, Cheng J, Chen FJ et al (2014) Gelatin functionalized graphene oxide for mineralization of hydroxyapatite: biomimetic and in vitro evaluation. Nanoscale 6(10):5315–5322. https://doi.org/10.1039/c4nr00355a
106. Ali A, Singh BN, Yadav S et al (2021) CuO assisted borate 1393B3 glass scaffold with enhanced mechanical performance and cytocompatibility: an In vitro study. J Mech Behav Biomed Mater 114:104231. https://doi.org/10.1016/j.jmbbm.2020.104231
107. Singh BN, Veeresh V, Mallick SP et al (2019) Design and evaluation of chitosan/chondroitin sulfate/nano-bioglass based composite scaffold for bone tissue engineering. Int J Biol Macromol 33:817–830. https://doi.org/10.1016/j.ijbiomac.2019.04.107
108. Kumar P, Dehiya BS, Sindhu A (2017) Comparative study of chitosan and chitosan–gelatin scaffold for tissue engineering. Int Nano Lett 7(4):285–290. https://doi.org/10.1007/s40089-017-0222-2
109. Zakhem E, Bitar KN (2015) Development of chitosan scaffolds with enhanced mechanical properties for intestinal tissue engineering applications. J Funct Biomater 6(4):999–1011. https://doi.org/10.3390/jfb6040999
110. Kuttappan S, Mathew D, Nair MB (2016) Biomimetic composite scaffolds containing bioceramics and collagen/gelatin for bone tissue engineering-a mini review. Int J Biol Macromol 93:1390–1401. https://doi.org/10.1016/j.ijbiomac.2016.06.043
111. Huang Y, Onyeri S, Siewe M et al (2005) In vitro characterization of chitosan–gelatin scaffolds for tissue engineering. Biomaterials 26:7616–7627. https://doi.org/10.1016/j.biomaterials.2005.05.036